STEM CELLS TRANSLATIONAL MEDICINE®

STANDARDS, POLICIES, PROTOCOLS, AND REGULATIONS FOR CELL-BASED THERAPIES

In Pursuit of Authenticity: Induced Pluripotent Stem Cell-Derived Retinal Pigment Epithelium for Clinical Applications

KIYOHARU J. MIYAGISHIMA,[a,*] QIN WAN,[a,*] BARBARA CORNEO,[c,*] RUCHI SHARMA,[b] MOSTAFA R. LOTFI,[a] NATHAN C. BOLES,[d] FANG HUA,[a] ARVYDAS MAMINISHKIS,[a] CONGXIAO ZHANG,[a] TIMOTHY BLENKINSOP,[e] VLADIMIR KHRISTOV,[a] BALENDU S. JHA,[b] OMAR S. MEMON,[a] SUNITA D'SOUZA,[f] SALLY TEMPLE,[d,†] SHELDON S. MILLER,[a,†] KAPIL BHARTI[b,†]

Key Words. Induced pluripotent stem cell (iPSC) • Retinal pigment epithelium • Cell authentication • Cellular therapy • Genetic differences

[a]Section on Epithelial and Retinal Physiology and Disease and [b]Unit on Ocular and Stem Cell Translational Research, National Eye Institute, National Institutes of Health, Bethesda, Maryland, USA; [c]Columbia Stem Cell Core Facility, Columbia University Medical Center, New York, New York, USA; [d]Neural Stem Cell Institute, Rensselaer, New York, USA; [e]Department of Development and Regenerative Biology and [f]Department of Pharmacology and Systems Therapeutics, Icahn School of Medicine at Mount Sinai, New York, New York, USA

[*]Co-first authors.

[†]Co-senior authors.

Correspondence: Kapil Bharti, Ph.D., National Institutes of Health, National Eye Institute, 10 Center Drive, MSC 2510, Bethesda, Maryland 20892, USA. Telephone: 301-451-9372; E-Mail: kapilbharti@nei.nih.gov

Received January 19, 2016; accepted for publication April 18, 2016; published Online First on July 11, 2016.

1066-5099/2016/$20.00/0

http://dx.doi.org/10.5966/sctm.2016-0037

ABSTRACT

Induced pluripotent stem cells (iPSCs) can be efficiently differentiated into retinal pigment epithelium (RPE), offering the possibility of autologous cell replacement therapy for retinal degeneration stemming from RPE loss. The generation and maintenance of epithelial apical-basolateral polarity is fundamental for iPSC-derived RPE (iPSC-RPE) to recapitulate native RPE structure and function. Presently, no criteria have been established to determine clonal or donor based heterogeneity in the polarization and maturation state of iPSC-RPE. We provide an unbiased structural, molecular, and physiological evaluation of 15 iPSC-RPE that have been derived from distinct tissues from several different donors. We assessed the intact RPE monolayer in terms of an ATP-dependent signaling pathway that drives critical aspects of RPE function, including calcium and electrophysiological responses, as well as steady-state fluid transport. These responses have key in vivo counterparts that together help determine the homeostasis of the distal retina. We characterized the donor and clonal variation and found that iPSC-RPE function was more significantly affected by the genetic differences between different donors than the epigenetic differences associated with different starting tissues. This study provides a reference dataset to authenticate genetically diverse iPSC-RPE derived for clinical applications. STEM CELLS TRANSLATIONAL MEDICINE *2016;5:1562–1574*

SIGNIFICANCE

The retinal pigment epithelium (RPE) is essential for maintaining visual function. RPE derived from human induced pluripotent stem cells (iPSC-RPE) offer a promising cell-based transplantation therapy for slowing or rescuing RPE-induced visual function loss. For effective treatment, iPSC-RPE must recapitulate the physiology of native human RPE. A set of physiologically relevant functional assays are provided that assess the polarized functional activity and maturation state of the intact RPE monolayer. The present data show that donor-to-donor variability exceeds the tissue-to-tissue variability for a given donor and provides, for the first time, criteria necessary to identify iPSC-RPE most suitable for clinical application.

INTRODUCTION

Induced pluripotent stem cells (iPSCs) are a valuable source for generating retinal pigment epithelium (RPE) for transplantation to alleviate visual impairment associated with age-related macular degeneration, a disease that afflicts 20 to 25 million people worldwide [1, 2]. On the basis of pioneering work done with in vitro RPE differentiation and with surgical techniques to transplant RPE monolayers in the eye [3–6], pluripotent stem cell-derived RPE is considered an ideal target for the development and optimization of stem cell therapy. However, generating stem cell-based therapy requires well-defined and authenticated iPSC-RPE [7].

The RPE is a monolayer of pigmented, hexagonal cells connected by tight junctions that compose part of the outer blood-retina barrier and that support photoreceptor function by the coordinated action of multiple regulatory mechanisms that act in and around the subretinal space (SRS) [8–16]. The highly polarized distribution of a cassette of apical and basolateral membrane ion channels, receptors, and transporters are essential for maintaining these specialized functions

and facilitating communication with adjacent photoreceptors [17–20]. For example, the light-induced ATP increase in the SRS activates calcium signaling within the RPE via apical membrane purinergic $P2Y_2$ receptors [19, 21]. Subsequent downstream signaling leads to the inhibition of apical membrane K^+ channels and the activation of basolateral membrane Cl^- channels that along with the appropriate counter ions osmotically drive fluid across the epithelium from the retinal to choroidal side of the tissue. In vivo, transitions between light and dark likely trigger the RPE purinergic response and require the coordination of multiple signaling pathways within the retina/RPE complex [19, 21–23]. The subsequent increase in fluid absorption helps regulate and maintain changes in SRS hydration, chemical composition, and retinal adhesion [19, 24–26].

To date, studies on the characterization of iPSC-derived RPE have focused on select protein biomarkers, gene expression, and limited functional assays. These studies are valuable but lack a direct comparison of the iPSC-derived RPE to the physiology of human fetal retinal pigment epithelium (hfRPE) that well mimic the native tissue and also respond in vitro to stimuli that accompany light onset/offset [10, 19, 25–34]. For example, Kamao et al. generated and characterized iPSC-RPE sheets that exhibited typical RPE protein markers, gene expression, and polarized growth factor secretion comparable to human fetal RPE [35]. Transplantation of iPSC-RPE sheets into the Royal College of Surgeons rat SRS increased outer nuclear layer thickness suggesting restoration of defective photoreceptor function in this retinal degeneration model. However, the physiology and immunoregulatory capacity of these cells remain largely unexplored. In another study, Brandl et al. measured vascular endothelial growth factor (VEGF)-A secretion and image-based phagocytosis in fibroblast-derived iPSC-RPE, but in these cell lines VEGF-A secretion was predominantly apical, suggesting that they had not attained proper polarization [36].

Kokkinaki et al. have made a relatively broad attempt to characterize iPSC-RPE polarity and function [37]. They performed image-based analysis of phagocytosis using fluorescent latex beads, polarized secretion of VEGF, and gene expression analysis of 89 genes selected for their expression in human fetal and adult RPE [32]. However, the author's claim that single-cell TTX-sensitive Na currents observed in their iPS-derived RPE represents a property of native tissue is controversial given the extensive prior evidence indicating that these currents are an artifact of cell culture and are not seen in native RPE [38, 39]. These experiments were performed on cells plated onto poly-D-lysine and laminin coated glass coverslips. It has been shown that under these culture conditions retinal pigment epithelial cells are unpolarized and lack hexagonal shape and pigmentation and consequently have a tendency to transdifferentiate into a neuronal phenotype [29, 39, 40].

In the present study, we have used multiple donors and tissues from these donors to estimate the amount of biological variation among iPSC clones and donors. Rather than limiting our analysis to single cells or to the collective ability of individual cells to perform RPE-like functions (e.g., phagocytosis), we employed functional assays (calcium imaging, electrophysiology, fluid transport) that closely assess the integrity of the intact monolayer. Focus is placed on the ATP-mediated purinergic pathway given its broad involvement in RPE physiology. Direct comparisons with previously well-characterized primary cultures of human RPE have been used to evaluate and rank the overall molecular, structural, and physiological properties of the iPSC-derived RPE from different clones and donors [33, 34]. Our goal is to provide an extensive functional assessment of intact RPE monolayers that can be used to benchmark differences attributed to donor and clonal variability and serve as a reference for authenticating RPE derived from any pluripotent stem cell source.

Materials and Methods

Immunostaining of iPSC-RPE Monolayers for RPE Protein Biomarkers

iPSC-RPE were washed three times with phosphate buffered saline Tween 20 (PBST) (0.5% Tween 20 in 1× phosphate buffered saline [PBS]), before fixing in 2% paraformaldehyde (PFA) for 20 minutes at room temperature (RT). Following three additional washes with PBST, cells were permeabilized with immunocytochemistry (ICC) blocking buffer (1× PBST, 0.5% bovine serum albumin [BSA], 0.5% Tween 20, 0.05% sodium azide, 0.1% Triton X-100) for 1 hour. RPE monolayers were incubated with primary antibodies against ezrin (E8897; 1:200; Sigma-Aldrich, St. Louis, MO, https://www.sigmaaldrich.com); collagen IV (ab6311; 1:100; Abcam, Cambridge, MA, www.abcam.com); ALDH1A3 (ab80176; 1:100; Santa Cruz Biotechnology, Santa Cruz, CA, http://www.scbt.com); and TYRP1 (ab89635; 1:100; Santa Cruz Biotechnology). Samples were left at RT for 1 hour followed by overnight incubation at 4°C. Samples were washed three times with PBST before adding appropriate Alexa Fluor 555 tagged secondary antibodies (1:1000; Thermo Fisher Scientific, Waltham, MA, www.thermofisher.com), Phalloidin 488 (1:200; catalog no. A12379; Thermo Fisher Scientific), and Hoechst (1:2000; catalog no. H3570; Thermo Fisher Scientific). Samples were dark incubated on a rocker for 1 hour. Following three washes with PBST, samples were mounted on a glass slide with Fluoromount-G aqueous mounting medium (catalog no. 0100-01; SouthernBiotech, Birmingham, AL, https://www.southernbiotech.com) and imaged with a Zeiss Axio Imager M2 microscope with Apotome 2 and Zen 2012 software (Carl Zeiss AG, Oberkochen, Germany, http://www.zeiss.com).

Quantitative Reverse Transcription-Polymerase Chain Reaction Analysis of mRNA and miRNA Expression

Total RNA was isolated using NucleoSpin RNA (catalog no. 740955; Machery-Nagel, Düren, Germany, http://www.mn-net.com) and microRNA was purified using mirVana miRNA isolation kit (Ambion; Thermo Fisher Scientific) per manufacturer's protocol. RNA and miRNA concentration was quantified using an ND-1000 spectrophotometer (Nanodrop Technologies, Wilmington, DE, http://www.nanodrop.com). Reverse transcription of mRNA to cDNA was performed using a SuperScript III First-Strand Synthesis kit (catalog no. 11904-018; Thermo Fisher Scientific) and miScript II RT Kit (Qiagen, Hilden, Germany, https://www.qiagen.com) was used for miRNA using manufacturer's instructions. The cDNA was diluted to working concentrations of 1 ng/μl. For gene expression, 2 ng of cDNA was loaded into each well with 4 μl of RT^2 SYBR Green qPCR Mastermix (catalog no. 330503; Qiagen) and water. Custom 359-gene plates were purchased and were developed using validated primer sets (catalog no. CAPH10484E; Qiagen). Quantitative polymerase chain reaction (qPCR) for miRNA was run using miScript SYBR Green PCR Kit (Qiagen) according to manufacturer's protocol on a ViiA 7 Real-Time

PCR System (Thermo Fisher Scientific). A custom miScript miRNA PCR Array (catalog no. CAIH0031E; Qiagen) included 88 miRNAs, which were grouped for analysis: RPE (23), retina (13), choroid (18), embryonic stem (ES) (21), and differentiation (13). Four house-keeping miRNAs (SNORD48, SNORD47, SNORD44, RNU6-2) were used as internal controls. Relative quantification was calculated using the $2^{-\Delta\Delta CT}$ method [41].

Intracellular Ca^{2+} Imaging

A ratiometric dye, Fura-2 AM (F1221; Molecular Probes; Thermo Fisher Scientific), was used to measure the intracellular free Ca^{2+} concentration in iPSC-RPE. Samples were incubated with 33 μM Fura-2 a.m. and 0.07% Pluronic F-127 (P3000MP; Molecular Probes; Thermo Fisher Scientific) at RT for 1 hour in ringer supplemented with 1 mM probenecid to block the efflux of the cytosolic dye. The dye-loaded samples were mounted into a modified Üssing chamber permitting independent perfusion of apical and basal bath. A polychrome V monochromator (TILL Photonics; FEI Life Sciences, Hillsboro, OR, http://www.fei.com) was used in conjunction with custom software written in LabVIEW to provide high speed photic excitation between 340 nm and 385 nm every 0.5 second and a photomultiplier tube measured the emission fluorescence at 510 nm.

Electrophysiological Recordings

RPE monolayer cultures derived from iPSC lines were mounted on a modified Üssing chamber as described previously for primary hfRPE [19, 22]. Calomel electrodes in series with Ringer's solutions and agar bridges were used to measure the transepithelial potential (TEP). The signals from intracellular microelectrodes were referenced to the basal bath to measure the basolateral membrane potential (V_b) and the apical membrane potential (V_a) was calculated by the equation: $V_a = V_b - TEP$. The total transepithelial resistance (R_t), and the ratio of the apical to basolateral membrane resistance (R_A/R_B) were obtained by passing 2–4 μA current pulses across the tissue and measuring the resultant changes in TEP, V_a, and V_b.

Fluid Transport Across iPSC-RPE Monolayer

Transepithelial fluid absorption rate (J_v) was measured using a capacitance probe (MTI Instruments, Albany, NY, http://www.mtiinstruments.com) technique as described previously [11, 16, 22, 33]. Fluid transport measurements were performed in minimal essential medium supplemented with 0.3% (w/v) taurine, hydrocortisone, triiodo-thyronin (THT). Briefly, RPE monolayers cultured on transwells were mounted in a modified Üssing chamber made of Kel-F and maintained in an incubator at 37°C with a humidity of 50%. The columns of fluid were topped with mineral oil and a floating Kel-F disc to reduce evaporation.

Statistical Analysis

All data were presented as mean +/− SEM and statistical analysis was performed using a two-tailed *t* test with 95% confidence interval. Data were considered significant at p values $< .05$.

Results

We generated 15 different iPSC lines from genetically and epigenetically diverse tissue sources with the goal to identify functional variation among iPSC-RPE and establish robust criteria for authenticating iPSC-RPE. Seven iPSC lines were derived from fetal ocular tissues (RPE or cornea) from the same donor. Eight lines were generated from three epigenetically distinct adult ocular tissues (RPE, cornea, or sclera) from three different donors (Table 1). Three genetically independent cultured confluent monolayers of hfRPE were included for comparison, because their physiology has been broadly analyzed and found to resemble native human RPE [31, 33, 42]. The iPSC lines in this study were characterized as pluripotent and were able to differentiate into all three germ layers (supplemental online Fig. 1A, 1B, 1C). Furthermore, irrespective of the starting tissue, all iPSC lines differentiated into RPE. Although the efficiency of differentiation varied, it was not correlated with tissue origin.

For all experiments, iPSC-RPE were cultured on semipermeable transwell membranes as confluent monolayers. All iPSC-RPE expressed the key RPE proteins EZRIN, COLLAGEN IV, TYRP1, and ALDH1A3 (representative lines shown in Fig. 1A). Ultrastructural comparisons were performed by transmission electron microscopy (TEM) (supplemental online Fig. 2). These initial experiments demonstrate that using the present techniques most RPE derived from different iPSCs are structurally and morphologically similar to each other, irrespective of genetic and epigenetic differences of the starting tissue sources.

Molecular Authentication of iPSC-RPE

The variation in mRNA and miRNA expression of the iPSC-RPE preparations was evaluated using previously published protocols to analyze expression of gene sets (163 RPE-signature genes, 89 adult RPE-specific genes, 71 fetal RPE-specific genes, and 21 developmental [non-RPE] genes) and miRNA sets (23 RPE-enriched miRNAs, 13 retina-enriched miRNAs, 18 choroid-enriched miRNAs, 21 stem cell-enriched miRNAs, and 13 differentiated cell-enriched miRNA) [31, 32, 43, 44] (supplemental online Fig. 3A– 3F). The expression levels represented as fold-change in each of the 15 iPSC-derived RPE samples were normalized relative to the expression data from hfRPE (supplemental online data).

Most iPSC-derived RPE are molecularly authentic and share similar levels of normalized mRNA and miRNA expression to each other and are within two- to fourfold of hfRPE. For each RPE sample, the mean expression of 89 adult RPE-specific genes (adult) and 71 fetal RPE-specific genes (fetal) are compared in a two-dimensional plot (Fig. 1B; supplemental online Fig. 3A, 3B). iPSC-RPE shared similar fetal gene expression to primary RPE (hfRPE1-3, black crosses); however, many lines displayed a more adult-like pattern (fR-iPSC-RPE1-1; fC-iPSC-RPE1-1,3; aS-iPSC-RPE3; aR-iPSC-RPE4-1,2). In addition, the gene expression profiles showed pronounced donor-to-donor and clone-to-clone variability. For example, aR-iPSC-RPE4-1,2 and aC-iPSC-RPE4-1 (orange solid/open squares) derived from one adult donor showed higher expression overall of both adult and fetal RPE-specific genes compared with iPSC-RPE from other donors (Fig. 1B), providing evidence for interdonor variability.

Consistent with this result, the expression profile of RPE signature versus developmental genes (Fig. 1C; supplemental online Fig. 3C, 3D) show that some iPSC-RPE (such as, aR-iPSC-RPE4-1,2 and aC-iPSC-RPE4-1) express higher levels of RPE signature genes that even further distinguish them from other cell types [32]. Lines derived from the same donor have minimal variance, for example, fR-iPSC-RPE1-1,2,3 (blue solid circles) derived from fetal RPE are similar in gene expression to fC-iPSC-RPE1-2,3 (empty

Table 1. Fifteen human iPSC lines were generated and differentiated into retinal pigment epithelium

iPSC lines[a]	iPSC clones after RPE differentiation[b]	Passage	Tissue source	Gender	Age, years
NSCI-BC1i-fR1	fR-iPSC-RPE1-1	14	fetal RPE	F	fetal
NSCI-BC1i-fR2	fR-iPSC-RPE1-2	12	fetal RPE		
NSCI-BC1i-fR3	fR-iPSC-RPE1-3	14	fetal RPE		
NSCI-BC1i-fR4	fR-iPSC-RPE1-4	13	fetal RPE		
NSCI-BC1i-fC1	fC-iPSC-RPE1-1	21	fetal cornea		
NSCI-BC1i-fC2	fC-iPSC-RPE1-2	25	fetal cornea		
NSCI-BC1i-fC3	fC-iPSC-RPE1-3	23	fetal cornea		
NSCI-BC2i-aR	aR-iPSC-RPE2	22	adult RPE	F	91
NSCI-BC2i-aC	aC-iPSC-RPE2	22	adult cornea		
NSCI-BC3i-aR	aR-iPSC-RPE3	24	adult RPE	M	63
NSCI-BC3i-aS	aS-iPSC-RPE3	23	adult sclera		
NSCI-BC4i-aR1	aR-iPSC-RPE4-1	29	adult RPE	F	71
NSCI-BC4i-aR2	aR-iPSC-RPE4-2	27	adult RPE		
NSCI-BC4i-aC1	aC-iPSC-RPE4-1	24	adult cornea		
NSCI-BC4i-aC2	aC-iPSC-RPE4-2	29	adult cornea		

[a]Nomenclature for iPSC lines: institute + researcher + donor number + induced pluripotent stem cell (i) + adult (a) or fetal (f) + RPE (R) or cornea (C) or sclera (S) + iPSC clone number.
[b]iPSC-derived RPE naming convention: Tissue information adult (a) or fetal (f) + RPE (R) or cornea (C) or sclera (S) + human iPSC-derived RPE (iPSC-RPE) + donor number + iPSC clone number.

blue circles) derived from the fetal cornea of the same donor. However, two additional iPSC-RPE from this same donor, fC-iPSC-RPE1-1 and fR-iPSC-RPE1-4, show significantly higher expression of developmental genes, additionally indicating clone-to-clone variation in iPSC-RPE. Closer examination of the developmental genes expressed in these two outliers revealed an upregulation of *KLF4* (44, 75-fold respectively) and *SOX2* (28-fold in fR-iPSC-RPE1-4), suggesting that these pluripotent genes were not completely silenced upon differentiation (supplemental online Fig. 3D).

MicroRNAs provide fine-tuned regulation of gene expression to control a stably differentiated cell fate. Specific miRNAs are expressed in pluripotent stem cells and in retinal pigment epithelial cells [31, 43, 45, 46]; therefore, we assessed whether iPSC-RPE exhibited developmental stage-specific miRNA expression that could be used to identify incompletely differentiated RPE. A comparison of the average ES cell-specific and differentiation-associated miRNAs confirmed that the majority of iPSC-RPE formed a tight cluster around the control hfRPE showing their close similarity in expression. ES cell-specific miRNAs were repressed to levels similar to primary hfRPE, consistent with maintenance of the differentiated state (Fig. 1D; supplemental online Fig. 3E). Two iPSC-RPE, fR-iPSC-RPE1-2 (blue solid circle) and fC-iPSC-RPE1-1 (blue open circle), continued to express significantly higher level of ES miRNAs (especially hsa-mir-302c, hsa-mir-367, and hsa-mir-371) as compared with hfRPE (Fig. 1D). The TEM for fC-iPSC-RPE1-1 (supplemental online Fig. 2) revealed an absence of apical processes and loss of typical epithelial morphology, consistent with its abnormal expression of developmental genes and ES cell-associated miRNAs (Fig. 1C, 1D).

Tissue-specific miRNAs play a role in maintaining tissue differentiation, identity, and function; therefore, we assessed the expression of previously published RPE, retina, and choroid-associated miRNAs [31]. As illustrated in Figure 1E, the profiles of most iPSC-RPE preparations are similar to primary hfRPE, whereas fR-iPSC-RPE1-2 and fC-iPSC-RPE1-1 show a distinct expression well apart from the other iPSC-RPE with higher expression of choroid and retina-associated miRNAs. Taken together, our results indicate that starting tissue and epigenetic status do not necessarily determine the expression of tissue-specific miRNAs in differentiated iPSC-RPE (supplemental online Fig. 3F).

Functional Authentication of iPSC-RPE

The RPE is one of the most active phagocytic cells in the body; its diurnal renewal of photoreceptor outer segments maintains the health and integrity of the distal retina [47, 48]. Phagocytic assays revealed that most of the iPSC-RPE were comparable to hfRPE, except for fC-iPSC-RPE1-2 and aR-iPSC-RPE3, which had significantly lower phagocytic capacity (supplemental online Fig. 4). These iPSC-RPE had not been identified previously as outliers by structural analysis or gene expression suggesting that evaluation of cellular function is a potential tool for discerning the quality of iPSC-RPE. The intactness of the epithelial sheet and the electrical activity of the RPE monolayer are essential for its function; thus, iPSC-RPE are more fully characterized by assessing the responses of confluent monolayers rather than individual cells [49]. Therefore, we expanded our functional analysis of the intact monolayer to several components of the ATP-mediated purinergic signaling pathway, critical elements in controlling the chemical composition and volume of the SRS [19, 22, 23, 50, 51]. Four representative iPSC-RPE were selected from the complete dataset to illustrate comparisons to hfRPE, two derived from adult donor-matched RPE and cornea, and two from fetal donor-matched RPE and cornea (Figs. 2–4). The full data set along with statistical analysis for all iPSC-RPE is

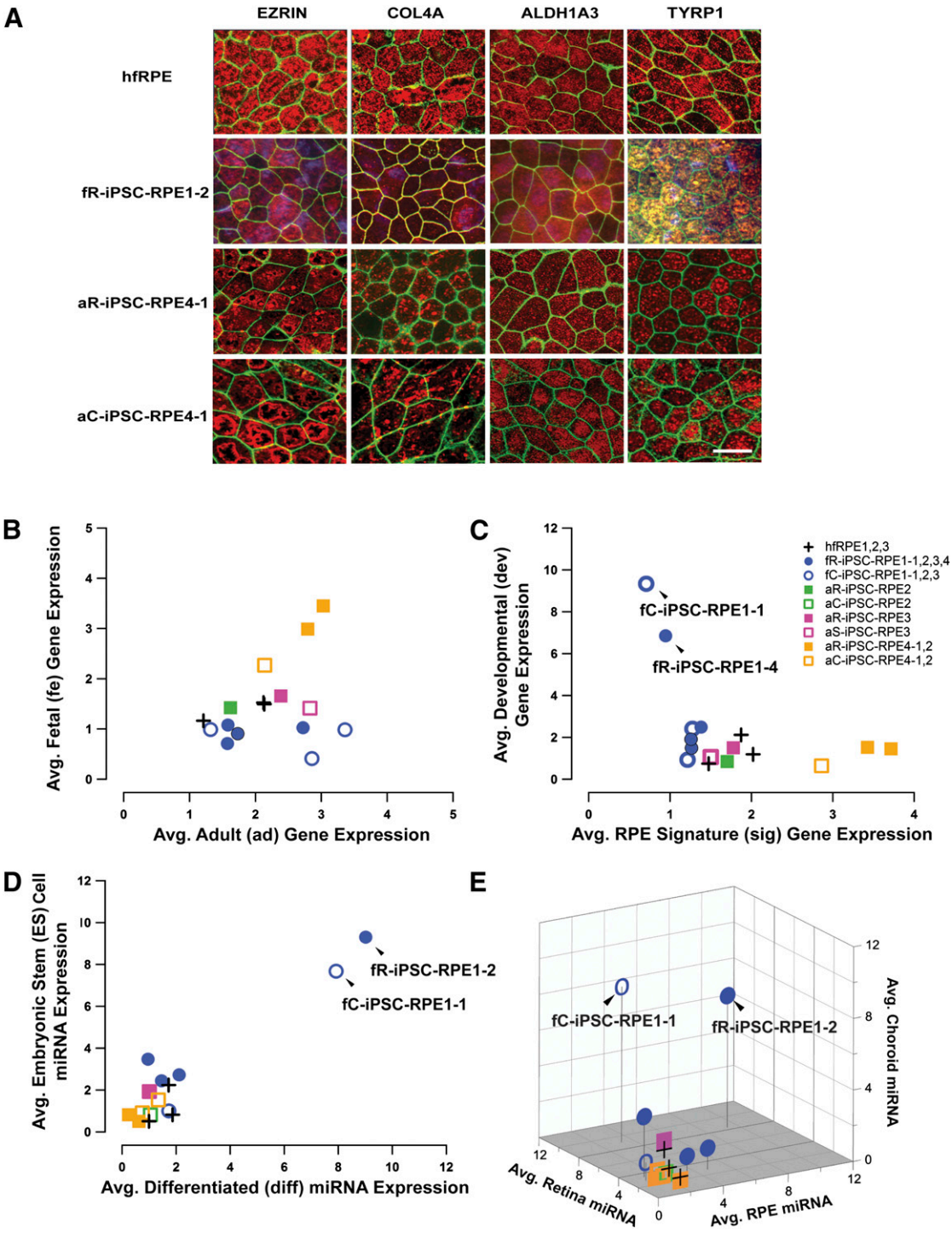

Figure 1. Signature protein markers and mRNA and miRNA expression profiles of iPSC-RPE. **(A):** Each image shows an en face view of the RPE monolayer immunostained for typical RPE markers with the maximum-intensity projection through the *z*-axis. RPE were stained with antibodies against an apical marker (EZRIN-red), a basal marker (COLLAGEN IV-red), a visual cycle protein (ALDH1A3-red), and a pigmentation protein (TYRP1-red). Phalloidin (green) was used to visualize cell boundary. Scale bar: 20 μm. **(B–E):** mRNA and miRNA expression. iPSC-RPE derived from different tissue sources are shown as (cross: hfRPE, circle: fetal, square: adult). Filled shapes denote RPE-derived iPSC-RPE, whereas open shapes denote cornea- or sclera-derived iPSC-RPE. Every donor is represented by a different color. Numerals at the end of each iPSC name distinguish the donors and are separated by a dash with numbers indicating different clones from that donor. iPSC-RPE that share similar expression cluster together and identify potential outliers. **(B):** Mean expression of adult RPE-specific genes is plotted against the mean expression of fetal RPE-specific genes. **(C):** Mean expression of RPE-signature genes (sig) plotted against developmental, non-RPE genes. **(D):** Mean expression of miRNAs associated with embryonic stem cells plotted against miRNAs associated with differentiated cells. **(E):** Mean expression of tissue-specific miRNAs represented in 3 axes, for RPE (*x*-axis), retina (*y*-axis), and choroid (*z*-axis). For corresponding heat maps, see supplemental online Figure 3. Abbreviations: Avg., average; hfRPE, human fetal retinal pigment epithelium; iPSC, induced pluripotent stem cell; RPE, retinal pigment epithelium.

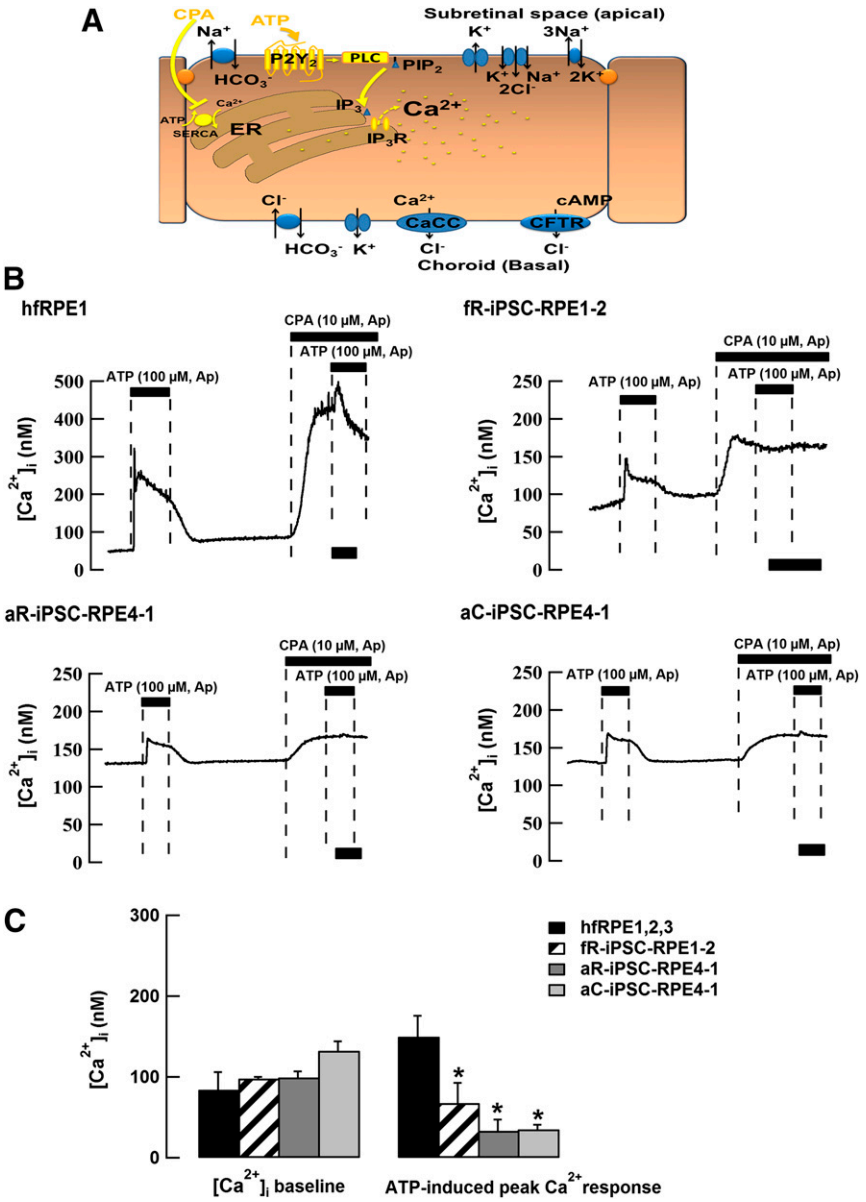

Figure 2. ATP-induced Ca^{2+} increase in human iPSC-RPE indicates intact Ca^{2+} signaling. **(A):** Schematic illustrating binding of ATP to purinergic receptors $P2Y_2$ on the RPE apical surface leads to an increase in cytosolic IP_3 and subsequent release of Ca^{2+} from the ER (shown in yellow). The inhibition of ER Ca^{2+}-ATPase with CPA prevents refilling of ER Ca^{2+} stores, thus blocking the ATP-evoked response, which is also affected by the polarized distribution of receptors, ion channels, and transporters including the apical membrane Na^+/K^+-ATPase, $Na^+/K^+/2Cl^-$ cotransporters, K^+ channels, and Na^+/HCO_3^- exchangers, as well as basolateral membrane CaCC, CFTR Cl^- channels, K^+ channels, and Cl^-/HCO_3^- exchangers. **(B):** Representative traces of ATP-induced Ca^{2+} responses in primary hfRPE or iPSC-RPE were obtained using the ratiometric dye Fura-2 a.m. In both primary hfRPE and iPSC-RPE, ATP induces a transient Ca^{2+} peak initiated by the ER Ca^{2+} release followed by a sustained plateau resulting from extracellular Ca^{2+} influx (possibly through Orai channels). CPA inhibits reuptake of Ca^{2+} into the ER and thus largely blocks the ATP-induced response. Black bars indicate duration of ATP or CPA application. Time scale bar: 2 minutes. Note: Data not available for fC-iPSC-RPE1-3. **(C):** Summary data for mean intracellular resting Ca^{2+} and the ATP-evoked peak Ca^{2+} increase for different iPSC-RPE. The measurements for each line were repeated at least three times and the data from three hfRPE donors were averaged as the control. $*p < .05$, indicating significant difference as compared with hfRPE control. See supplemental online Figure 5 and supplemental online Table 1 for additional information. Abbreviations: Ap, apical; CPA, cyclopiazonic acid; CaCC, Ca^{2+}-activated Cl^- channel; CFTR, cystic fibrosis transmembrane conductance regulator; ER, endoplasmic reticulum; hfRPE, human fetal retinal pigment epithelium; iPSC, induced pluripotent stem cell; RPE, retinal pigment epithelium.

shown in supplemental online Figures 5– 7 and supplemental online Tables 1– 3. The ATP pathway examined is initiated at the apical membrane by the activation of $P2Y_2$ receptors as schematically shown in Figures 2A–4A and includes the apical ATP-induced changes in (1) calcium signaling, (2) electrical responses, and (3) fluid transport.

As illustrated in Figure 2B, apical bath application of ATP in hfRPE induced a rapid initial increase in $[Ca^{2+}]_i$ followed by a sustained plateau that was blocked by CPA, an ER Ca^{2+} uptake inhibitor [19, 22]. Two parameters were used to authenticate iPSC-RPE across all 15 preparations: (1) baseline $[Ca^{2+}]_i$ of 80–120 nM and (2) ATP-evoked changes in $[Ca^{2+}]_i > 50$ nM [52–54]. Qualitatively,

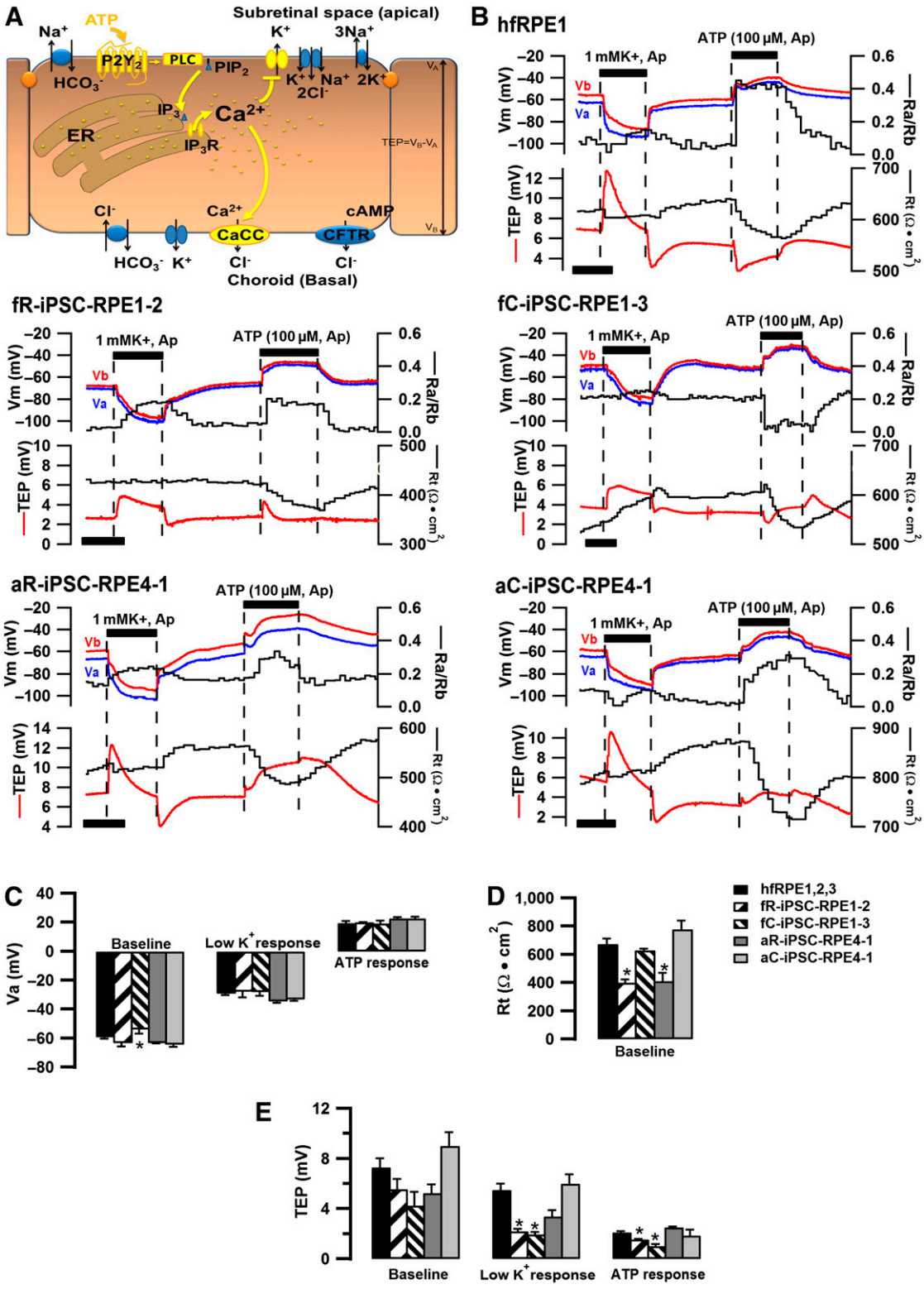

Figure 3. ATP-induced electrical responses in human iPSC-RPE. **(A):** The elevated cytosolic Ca^{2+} in response to ATP stimulation causes the activation of a basolateral membrane CaCC followed by a decrease in apical membrane K^+ conductance (shown in yellow), thus leading to electrical responses across the RPE monolayer. **(B):** Representative electrical responses of human iPSC-RPE to apical perfusion of low K^+ and ATP. For each graph, the top panel shows the changes of apical membrane potential (V_a, blue line), basolateral membrane potential (V_b, red line) and the ratio of apical to basal membrane resistance (R_a/R_b, black line); The bottom panel shows transepithelial potential (TEP, red line) and total tissue resistance (R_t, black line). V_a, V_b, R_a/R_b, TEP, and R_t were measured simultaneously in each experiment. The black horizontal bars indicate the time during which 1 mM K^+ or 100 μM ATP were perfused to the apical bath. Time scale bar: 5 minutes. Similar to the primary hfRPE,
(*Figure legend continues on next page*.)

ATP produced similar biphasic responses in all iPSC-RPE, suggesting that Ca^{2+} regulation is unaffected by genetic or epigenetic differences of the starting tissues used for iPSC generation (Fig. 2B). Furthermore, the baseline Ca^{2+} concentration of all iPSC-RPE was not statistically different from hfRPE (Fig. 2C). In contrast, the magnitude of the ATP-induced peak Ca^{2+} response varied across preparations (nM): hfRPE (149.8 $\pm$ 25.8; n = 11), fR-iPSC-RPE1-2 (73 $\pm$ 7.9; n = 6), aR-iPSC-RPE4-1 (33.5 $\pm$ 6.0; n = 4), and aC-iPSC-RPE4-1 (35.5 $\pm$ 2.5; n = 2). There were also significant differences between different donors (e.g., fR-iPSC-RPE1-2 vs. aR-iPSC-RPE4-1; p = .004), but not between iPSC-RPE derived from donor-matched tissues (e.g., aR-iPSC-RPE4-1 vs. aC-iPSC-RPE4-1; Fig. 2C). Two lines not previously identified as outliers, aR-iPSC-RPE2 and aC-iPSC-RPE2, displayed Ca^{2+} responses less than 30 nM suggesting a deficiency in the regulation of ER Ca^{2+} homeostasis (supplemental online Fig. 5; supplemental online Table 1). Thus donor-specific changes in $[Ca^{2+}]_i$ can be used to assess the authenticity of iPSC-RPE epithelia.

Intracellular recordings of RPE membrane potential in response to apical ATP or a small decrease in apical $[K^+]_o$ provide another independent assessment to authenticate RPE physiology. In hfRPE, apical ATP induced a membrane depolarization, accompanied by reduction in TEP and transepithelial resistance (R_t) (Fig. 3B). Altering the apical bath K^+ concentration from 5 to 1 mM mimics the extracellular K^+ drop that occurs in vivo in the SRS, which is initiated by changes in photoreceptor activity following the transition from dark-to-light [55]. In vitro, this K^+ decrease hyperpolarizes the RPE apical membrane, increases TEP, and decreases R_t (Fig. 3B).

Single cell recordings of membrane potential following the addition of apical ATP or low K^+ were practically indistinguishable in iPSC-RPE and control hfRPE (Fig. 3C; supplemental online Fig. 6). In contrast, the R_t and TEP measurements assess the integrity of the entire polarized monolayer and thus were able to identify subtle differences between different samples. Most (13/15) of the iPSC-RPE lines possessed R_t $>$300 $\Omega \cdot cm^2$, indicating tight junction integrity and an intact epithelial barrier function (Fig. 3D). We also found that TEP was highly variable across all iPSC-RPE with the baseline ranging from 2–10 mV, whereas the stimulated TEP responses to K^+ and ATP varied from 1–8 mV and 0.5–5 mV, respectively. Overall, differences in baseline or stimulated TEP responses were not attributed to the starting tissue from which iPSC-RPE were derived (fR vs. fC, n = 3; or aR vs. aC, n = 3; $p > .05$), suggesting negligible epigenetic influence on RPE electrical properties. We also observed donor-dependent TEP differences comparing across similar types of tissues in both the K^+ response, fC vs. aC (p = .01; n = 3), and in the ATP response, fR vs. aR (p = .04; n = 3) (Fig. 3E). As in the gene expression data, variability was observed between RPE derived from different iPSC clones generated from the same donor fR-iPSC-RPE1-1,3,4 (supplemental online Fig. 6; supplemental online Table 2). Therefore, the electrical recordings can identify subtle differences among different iPSC-RPE and thus provide a consistent set of parameters to authenticate iPSC-RPE.

Steady-state fluid transport across the intact epithelial monolayer is osmotically driven by active anion transport, accompanied by an appropriate counter ion, and mediated by a wide variety of cell signaling pathways following the ATP-induced activation of apical membrane $P2Y_2$ receptors (Fig. 4A). We measured apical-to-basal fluid absorption in all 15 iPSC-RPE following activation of the apical membrane $P2Y_2$ receptors by ATP (Fig. 4A). Representative hfRPE and iPSC-RPE traces are shown in Figure 4B. In hfRPE, steady-state J_v was 6.7 $\pm$ 1.2 μl/hour/cm^2 and apical ATP enhanced this absorption rate by approximately 50% (n = 18).

The steady-state J_v for the selected iPSC-RPE were all comparable to hfRPE and similar between preparations derived from epigenetically distinct tissues from the same donor (Fig. 4C). ATP induced a significant increase in fluid absorption in hfRPE (3.1 $\pm$ 0.6 μl/hour/cm^2; n = 18) and this increase was also observed in three of the four iPSC-RPE: fR-iPSC-RPE1-2, aR-iPSC-RPE-4-1, and aC-iPSC-RPE4-1.

Similar to the Ca^{2+} and electrical measurements, donor and clonal variation was predominant as compared with the epigenetic influence of the starting tissue (supplemental online Fig. 7; supplemental online Table 3). These results were independently corroborated using epinephrine to activate apical membrane α1-adrenergic receptors (data not shown) and increase net salt and fluid absorption across the RPE monolayer [16]. Bumetanide inhibition of the apical membrane Na, K, 2Cl cotransporter blocked the epinephrine-induced fluid transport across the RPE [56, 57]. Based on these results we conclude that the measurement of fluid flow from the apical to basal side of the RPE monolayer is a sensitive and informative assay to authenticate iPSC-RPE polarization and function.

Discussion

Our work provides a thorough dataset for authenticating iPSC-RPE and for determining the variations between genetically matched clones and between allelic heterogeneous starting tissues. As iPSC-RPE have the potential to provide an autologous or allogeneic cell-based replacement therapy, it is essential to establish acceptable limits of variability and to provide criteria for equivalence among iPSC-RPE derived from different individuals. The variability could result from four sources: (1) donor-to-donor/allelic variability, (2) retention of epigenetic memory, (3) clone-to-clone variability, and (4) the degree to which each iPSC-RPE resembles primary human fetal RPE. In this study we present detailed gene expression, structural, and functional analysis of 15 iPSC-RPE derived from different donors and tissues to systematically assess variability in RPE authentication. The heat map in Figure 5 is a semi-quantitative summary that ranks the outcomes of all the assays.

Taking all the criteria into consideration, only 20% of iPSC-RPE have a subpar assigned ranking less than 3 (fC-iPSC-RPE1-1,

(*Figure legend continued from previous page*.)
iPSC-RPE responded with membrane hyperpolarization when apical K^+ concentration was reduced to 1 mM and with membrane depolarization when ATP was added to the apical bath. **(C):** Summary data for V_a baseline and low K^+/ATP-induced V_a changes. (**D):** Summary data for R_t baseline. **(E):** Summary data for TEP baseline and low K^+/ATP-induced TEP changes. The measurements for each line were repeated at least three times and the data from three hfRPE donors were averaged as the control. $*p < .05$, indicating significant difference as compared with hfRPE control. See supplemental online Figure 6 and supplemental online Table 2 for additional information. Abbreviations: Ap, apical; CaCC, Ca^{2+}-activated Cl^- channel; CFTR, cystic fibrosis transmembrane conductance regulator; hfRPE, human fetal retinal pigment epithelium; iPSC, induced pluripotent stem cell; RPE, retinal pigment epithelium; TEP, transepithelial potential.

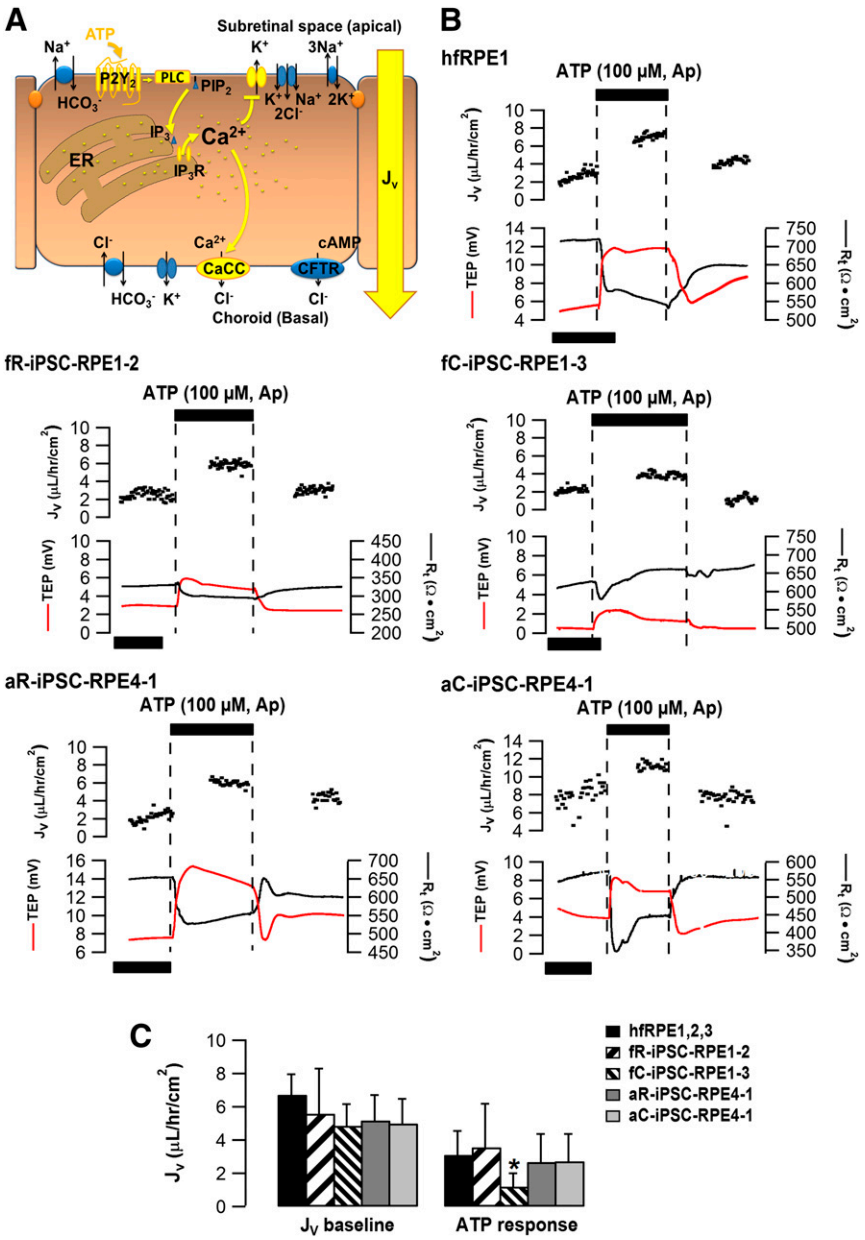

Figure 4. ATP-induced transepithelial fluid transport across human iPSC-RPE. **(A):** ATP stimulation elevates intracellular Ca^{2+} levels and activates CaCC on the RPE basolateral membrane. The movement of Cl^- from the subretinal space toward the choroid helps drive osmotically obliged transport of fluid across the RPE monolayer (shown in yellow). **(B):** Representative traces of steady-state transepithelial fluid absorption mediated by ATP in hfRPE or iPSC-RPE. Net fluid absorption (J_v, black dots) across the RPE is plotted as a function of time in the top panel of each graph. TEP (red line) and total tissue resistance (R_t, black line) are located in the bottom panel of each graph. Similar to the primary hfRPE, addition of 100 μM ATP to the apical bath produced an increase in J_v accompanied with TEP increase and R_t decrease in all iPSC-RPE. Time scale bar: 50 min. **(C):** Summary data of J_v baselines and ATP-induced J_v responses for different iPSC-RPE. Data from three hfRPE donors were averaged as the control. *$p < .05$, indicating significant difference as compared with hfRPE control. See supplemental online Figure 7 and supplemental online Table 3 for additional information. Abbreviations: Ap, apical; CaCC, Ca^{2+} activated Cl^- channel; CFTR, cystic fibrosis transmembrane conductance regulator; hfRPE, human fetal retinal pigment epithelium; iPSC, induced pluripotent stem cell; RPE, retinal pigment epithelium; TEP, transepithelial potential.

aR-iPSC-RPE3, aS-iPSC-RPE3). Conversely, several other iPSC-RPE can be considered completely authentic based on their molecular and functional properties. Their identification is based on the authentication measures highlighted in yellow in Figure 5 and on the coordinated action of the ATP responses. The following three preparations were selected as optimal based on their overall evaluation score of greater than 4, and the requirement that each individual assay scored 3 or higher for each clone: aC-iPSC-RPE4-1, fC-iPSC-RPE1-2, and fR-iPSC-RPE1-3. These assays provide our most sensitive evaluation of RPE polarity to date and can sensitively distinguish differences between iPSC-RPE and, thus, extend the detection limit of genetic and structural data.

Our data also demonstrate that the function of iPSC-RPE and primary hfRPE are closely aligned and that most of the variation among different iPSC-RPE is contributed by allelic and clonal variation. Additional comparisons can be made between our

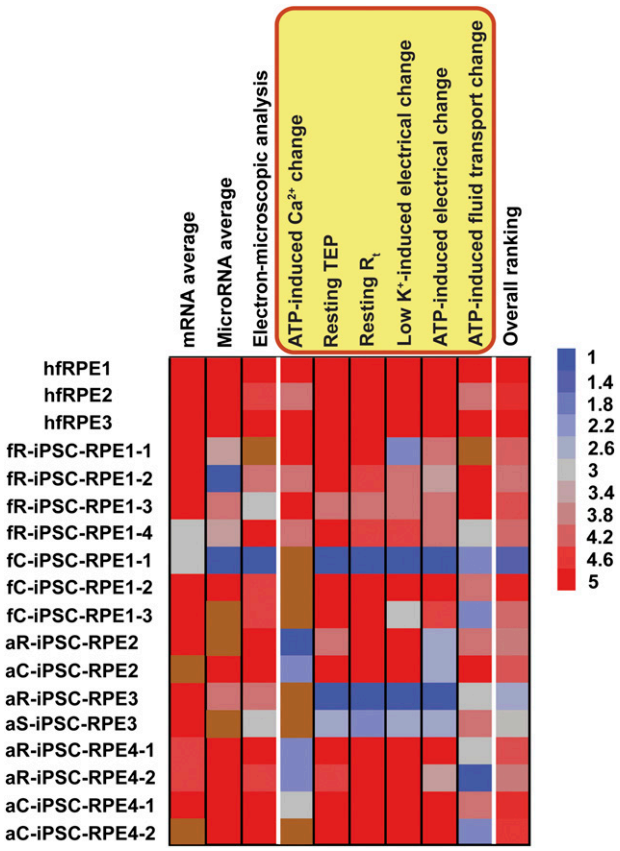

Figure 5. Ranking of overall performance of 15 iPSC-RPE preparations. mRNA and miRNA expression were normalized to hfRPE and ranked by their enrichment profiles. Functional assays were quantitatively scored relative to the physiological responses obtained from hfRPE. A nominal scale (1–5) was used to evaluate the iPSC-RPE lines, where 5 (denoted red) most closely resembles hfRPE, whereas 1 (denoted blue) bears least resemblance. Brown indicates that the data are not available. The heat map provides a graphical summary of the variability implicit in iPSC-derived RPE. iPSC-RPE with collectively low scores (lower than 3 subpar performing categories, denoted in blue) indicate inadequate attainment of the RPE phenotype (e.g., fC-iPSC-RPE3-1 and aR-iPSC-RPE5). Taking all the criteria into consideration, 20% have an overall subpar assigned ranking (less than 3, denoted blue). Abbreviations: hfRPE, human fetal retinal pigment epithelium; iPSC, induced pluripotent stem cell; RPE, retinal pigment epithelium.

iPSC-RPE results with those previously reported for cultures of adult RPE stem cell-derived RPE (RPESC-RPE) and native adult RPE [34]. Adult RPESC-RPE express the key characteristic features of native RPE but possessed lower transepithelial potential (1.19 $\pm$ 0.24 mV) and transepithelial resistance (178.7 $\pm$ 9.9 $\Omega \cdot cm^2$) compared with hfRPE and to the iPSC-RPE used in the present study.

We find no evidence that donor age or epigenetic memory in iPSCs affect the physiology or maturation state of derived RPE. These results help corroborate recent studies showing that epigenetic memory of iPSCs does not alter their differentiation capability [58, 59].

Most iPSC lines used in this study were similarly pluripotent and had a similar in vitro capability to differentiate into all three germ layers. iPSCs were selected for differentiation into RPE between passages 12 to 29 in an attempt to establish a safe cutoff to avoid genomic changes associated with very early or very late passages resulting in higher incidences of copy number variants that may affect the physiology of resulting cells [60, 61]. Although extended passaging has been reported to increase neural differentiation efficiency from iPSCs and enhance their functional profiles [62], there was no indication that extended passaging of iPSCs (e.g., aR-iPSC-RPE4-1 [p29], aC-iPSC-RPE4-2 [p29], fC-iPSC-RPE1-2 [p25]) resulted in increased efficiency of RPE differentiation or epithelial function compared with earlier passages (e.g., fR-iPSC-RPE1-2 [p12], fR-iPSC-RPE1-3 [p14], fR-iPSC-RPE1-4 [p13]).

A post hoc chromosomal analysis of our iPSC lines revealed mostly normal karyotypes; however, two lines (NSCI-BC3i-aR, NSCI-BC3i-aS) presented major chromosomal abnormalities (monosomy X and an unbalanced karyotype with a derivative chromosome 20). Although their gene and miRNA expression appeared normal, these abnormalities are consistent with their poor performance in our functional analysis. Variable X-chromosome inactivation in female iPSC or reactivation in iPSC derivatives has been suggested to change their differentiation capability or cellular phenotype [63, 64]. Within the 13 female-derived iPSC lines, we did not observe any significant variability in RPE differentiation or functionality. Thus, the potential variability in X-inactivation status following cellular differentiation did not lead to changes in the RPE-specific phenotype.

Previously, Hu et al. used a spontaneous differentiation strategy to demonstrate that some iPSC lines generated from primary human fetal RPE had a higher tendency to differentiate back into RPE-like cells as compared with iPSC lines derived from non-RPE sources [65]. However, the iPSC lines compared in their study were not genetically identical, differentiated with variable efficiency, and lacked extensive functional analysis of iPSC-RPE. The reproducibility of our differentiation protocol enabled us to demonstrate low donor-matched variation between iPSC-RPE from different starting tissues suggesting limited epigenetic influence.

In contrast, our gene expression and physiology results revealed higher donor-to-donor variability. In accordance with our data, Kajiwara et al. also demonstrated that the genetic background of individual donors had a strong impact on the propensity of human iPSC clones for hepatic differentiation [66]. Comparing 28 human iPSC lines originated from various somatic cells, they found that the variations in hepatic differentiation are largely attributed to donor differences, rather than the types of the original cells [66]. Given that RPE differentiation was always initiated around similar iPSC passages (Table 1), the higher donor variability suggests the existence of allelic differences in the rate and extent to which iPSC-RPE from different donors attain an RPE-phenotype in vitro.

Thus, to fully authenticate iPSC-RPE it was necessary to use a set of assays that would additionally assess the varying degrees of polarization of the intact RPE monolayer. We first analyzed the mRNA/miRNA expression, protein localization and structural characteristics of each iPSC-RPE; these methods have commonly been used as authentication criteria for iPSC-RPE. The compactness of the gene expression data suggests that most of the lines were fully differentiated and that the epigenetic differences in starting tissue are not a major determinant of RPE phenotype. We observed no apparent difference in immunofluorescence staining for mature RPE makers between iPSC-RPE and primary

hfRPE. TEM imaging provided information regarding the localization of key subcellular structures but was limited by small sampling size and the presence of microtome cutting artifacts. Assessing phagocytic capability provided evidence that cellular functionality of retinal pigment epithelial cells was an important component of authentication. However, it is an insensitive cellular assay as it evaluates the collective phagocytic ability of individual cells and does not assess the polarization and maturation of the confluent monolayer. For example, aS-iPSC-RPE3 showed normal phagocytic capability (supplemental online Fig. 4), but TEM images revealed multiple cell layers (supplemental online Fig. 2) consistent with low TEP and R_t in our physiological assays (supplemental online Fig. 6; supplemental online Table 2). Thus, relying on phagocytosis as the only functional readout can be misleading and should be complemented by other physiological assays to authenticate iPSC-RPE.

For example, in Figure 1D, fR-iPSC-RPE1-2 exhibits differential expression of ES-associated miRNAs compared with hfRPE, but these differences are undetected in the developmental and fetal gene expression analysis. In contrast, fR-iPSC-RPE1-4 (another clone from the same donor) shows higher expression of developmental genes compared with hfRPE, but fetal gene and ES-associated miRNA expression characteristic of hfRPE. These differences highlight clone-to-clone variability and further underscore the importance of including assays that more globally assess the functional characteristics of the entire RPE monolayer. In accordance with this, we found that measuring ATP-induced changes in intracellular Ca^{2+}, membrane electrical responses, and fluid transport, concomitant with TEP and R_t in each assay, provided an accurate measure of iPSC-RPE functional responses to physiologically relevant stimuli.

The three functional measurements of the ATP-mediated responses assess the interactions of multiple proteins within the confluent electrically intact monolayer including protein expression, subcellular localization, protein-protein interaction, and intactness of signaling pathways. Activation by ATP mimics light onset and is therefore a critical sentinel of RPE health [22, 67]. Whereas outliers can be identified by uncharacteristic TEP, R_t, calcium, or J_v responses, relatively small differences specify normal donor-to-donor and technical variation. For example, variability exists in the baseline resistances of all iPSC-derived RPE independent of the starting tissue (RPE or cornea, supplemental online Table 2). Similar to hfRPE, most (12 of 15) of the iPSC-RPE possessed baseline resistances (R_t) $>300\,\Omega\cdot\mathrm{cm}^2$. Using the ATP mediated responses to provide further discrimination between iPSC-derived RPE, most iPSC-RPE could be characterized as authentic.

These measurements can be reproduced in other laboratories using commercially available diagnostic tools such as the EVOM2 (World Precision Instruments, Sarasota, FL, https://www.wpiinc.com) and EasyMount Ussing Chamber System (Physiologic Instruments, San Diego, CA, http://www.physiologicinstruments.com) that can provide assessment of TEP and R_t as quantitative and functional markers of RPE authenticity. Low cost live-cell Ca^{2+} imaging equipment is also widely available and can be easily implemented. As shown in Figure 5, cell-based assays that closely mimic physiological responses of the RPE monolayer provide the most sensitive functional readout of the state of the RPE. Active ion-linked fluid transport integrates a broad array of RPE activities that include the continual synthesis of signaling pathway proteins, tight junction, and plasma membrane proteins. This deeply coordinated set of events is fundamentally important for the maintenance of retinal pigment epithelial cell polarization, vectorial transport, and the homeostatic control of volume and chemical composition in and around the RPE following transitions between light and dark. Taken together, these functional assays (calcium imaging, electrophysiology, fluid transport) provide a sensitive metric to authenticate iPSC-RPE as a clinical product and to validate the manufacturing process for iPSC-RPE.

Conclusion

iPSC lines are capable of differentiating into authentic RPE that can be fully characterized by combining structural, molecular, and physiologically relevant functional assays to determine their suitability for transplantation. In these 15 iPSC-RPE, interdonor variance exceeds intradonor or epigenetic variance. This study establishes acceptable limits of variability among iPSC-RPE derived from different individuals. Based on the present data (selection criteria described above), we determined that the following RPE samples are optimal: aC-iPSC-RPE4-1, fC-iPSC-RPE1-2, and fR-iPSC-RPE1-3. These iPSC-RPE are from different aged donors and tissues, again illustrating no apparent epigenetic dependence on retinal pigment epithelial cell fate. We found that functional assays using the underlying signaling pathway molecules that mediate transepithelial fluid transport, driven by apical membrane purinergic or adrenergic receptors, provide the most sensitive readout of RPE polarization and authentication as they constitute a large set of proteins distributed throughout the monolayer that concomitantly regulate intracellular pH, calcium, and cell volume in and around the subretinal space. This set of physiological assays provides a necessary measure of RPE authenticity and an invaluable resource for transitioning iPSC-RPE to the clinic.

Acknowledgments

This study was supported by National Eye Institute Intramural Funds, NIH Center for Regenerative Medicine, and NIH Common Fund Grants to K.B. and S.M. Production and characterization of iPSCs was supported by National Institute of Aging Grant 1RF1AG042932-01 to S.T. and B.C. We thank Gretchen Kusek, Rachel Wurster, Natalia Lowry, and Carol Charniga (Sally Temple lab) for technical assistance and Dr. Peter Munson for statistical consultation.

Author Contributions

K.J.M. and Q.W.: collection and/or assembly of data, data analysis and interpretation, manuscript writing; B.C., R.S., M.R.L., N.C.B., F.H., A.M., C.Z., T.B., V.K., B.S.J., O.S.M., and S.D.: collection and/or assembly of data, data analysis and interpretation; S.T. and S.S.M.: conception and design, financial support; K.B.: conception and design, final approval of manuscript, financial support.

Disclosure of Potential Conflicts of Interest

S.T. is an employee of and has uncompensated stock options from Athghin Biotech and has uncompensated intellectual property rights. The other authors indicated no potential conflicts of interest.

REFERENCES

1 Chopdar A, Chakravarthy U, Verma D. Age related macular degeneration. BMJ 2003;326: 485–488.

2 Croze RH, Clegg DO. Differentiation of pluripotent stem cells into retinal pigmented epithelium. Dev Ophthalmol 2014;53:81–96.

3 Schwartz SD, Regillo CD, Lam BL et al. Human embryonic stem cell-derived retinal pigment epithelium in patients with age-related macular degeneration and Stargardt's macular dystrophy: Follow-up of two open-label phase 1/2 studies. Lancet 2014;385:509–516.

4 Nazari H, Zhang L, Zhu D et al. Stem cell based therapies for age-related macular degeneration: The promises and the challenges. Prog Retin Eye Res 2015;48:1–39.

5 Forest DL, Johnson LV, Clegg DO. Cellular models and therapies for age-related macular degeneration. Dis Model Mech 2015;8: 421–427.

6 Alvarez Palomo AB, McLenachan S, Chen FK et al. Prospects for clinical use of reprogrammed cells for autologous treatment of macular degeneration. Fibrogenesis Tissue Repair 2015;8:9.

7 French A, Bravery C, Smith J et al. Enabling consistency in pluripotent stem cell-derived products for research and development and clinical applications through material standards. STEM CELLS TRANSLATIONAl MEDICINE 2015; 4:217–223.

8 Strauss O. The retinal pigment epithelium in visual function. Physiol Rev 2005;85: 845–881.

9 Miller SS, Edelman JL. Active ion transport pathways in the bovine retinal pigment epithelium. J Physiol 1990;424:283–300.

10 Miller S, Maminishkis A, Li R et al. Retinal pigment epithelium: Cytokine modulation of epithelial physiology. In: Besharse J, Dana R, Dartt DA, eds. Encyclopedia of the Eye. 1st ed. Cleveland, OH: Academic Press, 2010:2344.

11 Shi G, Maminishkis A, Banzon T et al. Control of chemokine gradients by the retinal pigment epithelium. Invest Ophthalmol Vis Sci 2008;49:4620–4630.

12 LaVail MM. Circadian nature of rod outer segment disc shedding in the rat. Invest Ophthalmol Vis Sci 1980;19:407–411.

13 LaVail MM. Rod outer segment disc shedding in relation to cyclic lighting. Exp Eye Res 1976;23:277–280.

14 Lamb TD, Pugh EN Jr. Dark adaptation and the retinoid cycle of vision. Prog Retin Eye Res 2004;23:307–380.

15 Redmond TM, Yu S, Lee E et al. Rpe65 is necessary for production of 11-cis-vitamin A in the retinal visual cycle. Nat Genet 1998;20: 344–351.

16 Edelman JL, Miller SS. Epinephrine stimulates fluid absorption across bovine retinal pigment epithelium. Invest Ophthalmol Vis Sci 1991;32:3033–3040.

17 Mitchell CH, Reigada D. Purinergic signalling in the subretinal space: A role in the communication between the retina and the RPE. Purinergic Signal 2008;4:101–107.

18 Rosenthal R, Strauss O. Ca2+-channels in the RPE. Adv Exp Med Biol 2002;514:225–235.

19 Peterson WM, Meggyesy C, Yu K et al. Extracellular ATP activates calcium signaling, ion, and fluid transport in retinal pigment epithelium. J Neurosci 1997;17:2324–2337.

20 Li R, Wen R, Banzon T et al. CNTF mediates neurotrophic factor secretion and fluid absorption in human retinal pigment epithelium. PLoS One 2011;6:e23148.

21 Ho T, Jobling AI, Greferath U et al. Vesicular expression and release of ATP from dopaminergic neurons of the mouse retina and midbrain. Front Cell Neurosci 2015;9:389.

22 Maminishkis A, Jalickee S, Blaug SA et al. The P2Y(2) receptor agonist INS37217 stimulates RPE fluid transport in vitro and retinal reattachment in rat. Invest Ophthalmol Vis Sci 2002; 43:3555–3566.

23 Quinn RH, Miller SS. Ion transport mechanisms in native human retinal pigment epithelium. Invest Ophthalmol Vis Sci 1992;33: 3513–3527.

24 Botchkin LM, Matthews G. Chloride current activated by swelling in retinal pigment epithelium cells. Am J Physiol 1993; 265:C1037–C1045.

25 Adorante JS, Miller SS. Potassium-dependent volume regulation in retinal pigment epithelium is mediated by Na,K,Cl cotransport. J Gen Physiol 1990;96:1153–1176.

26 Bialek S, Miller SS. K^+ and Cl^- transport mechanisms in bovine pigment epithelium that could modulate subretinal space volume and composition. J Physiol 1994;475:401–417.

27 Adijanto J, Banzon T, Jalickee S et al. CO2-induced ion and fluid transport in human retinal pigment epithelium. J Gen Physiol 2009;133: 603–622.

28 Liao JL, Yu J, Huang K et al. Molecular signature of primary retinal pigment epithelium and stem-cell-derived RPE cells. Hum Mol Genet 2010;19:4229–4238.

29 Sonoda S, Spee C, Barron E et al. A protocol for the culture and differentiation of highly polarized human retinal pigment epithelial cells. Nat Protoc 2009;4:662–673.

30 Sonoda S, Sreekumar PG, Kase S et al. Attainment of polarity promotes growth factor secretion by retinal pigment epithelial cells: relevance to age-related macular degeneration. Aging (Albany, NY) 2009;2:28–42.

31 Wang FE, Zhang C, Maminishkis A et al. MicroRNA-204/211 alters epithelial physiology. FASEB J 2010;24:1552–1571.

32 Strunnikova NV, Maminishkis A, Barb JJ et al. Transcriptome analysis and molecular signature of human retinal pigment epithelium. Hum Mol Genet 2010;19:2468–2486.

33 Maminishkis A, Chen S, Jalickee S et al. Confluent monolayers of cultured human fetal retinal pigment epithelium exhibit morphology and physiology of native tissue. Invest Ophthalmol Vis Sci 2006;47:3612–3624.

34 Blenkinsop TA, Saini JS, Maminishkis A et al. Human adult retinal pigment epithelial stem cell-derived RPE monolayers exhibit key physiological characteristics of native tissue. Invest Ophthalmol Vis Sci 2015;56:7085–7099.

35 Kamao H, Mandai M, Okamoto S et al. Characterization of human induced pluripotent stem cell-derived retinal pigment epithelium cell sheets aiming for clinical application. Stem Cell Rep 2014;2:205–218.

36 Brandl C, Zimmermann SJ, Milenkovic VM et al. In-depth characterisation of Retinal Pigment Epithelium (RPE) cells derived from human induced pluripotent stem cells (hiPSC). Neuromolecular Med 2014;16:551–564.

37 Kokkinaki M, Sahibzada N, Golestaneh N. Human induced pluripotent stem-derived retinal pigment epithelium (RPE) cells exhibit ion transport, membrane potential, polarized vascular endothelial growth factor secretion, and gene expression pattern similar to native RPE. STEM CELLS 2011;29:825–835.

38 Botchkin LM, Matthews G. Voltage-dependent sodium channels develop in rat retinal pigment epithelium cells in culture. Proc Natl Acad Sci USA 1994;91:4564–4568.

39 Wen R, Lui GM, Steinberg RH. Expression of a tetrodotoxin-sensitive Na+ current in cultured human retinal pigment epithelial cells. J Physiol 1994;476:187–196.

40 Reh TA, Nagy T, Gretton H. Retinal pigmented epithelial cells induced to transdifferentiate to neurons by laminin. Nature 1987; 330:68–71.

41 Schmittgen TD, Lee EJ, Jiang J et al. Real-time PCR quantification of precursor and mature microRNA. Methods 2008;44:31–38.

42 Hernandez EV, Hu JG, Frambach DA et al. Potassium conductances in cultured bovine and human retinal pigment epithelium. Invest Ophthalmol Vis Sci 1995;36:113–122.

43 Tiscornia G, Izpisúa Belmonte JC. MicroRNAs in embryonic stem cell function and fate. Genes Dev 2010;24:2732–2741.

44 Houbaviy HB, Murray MF, Sharp PA. Embryonic stem cell-specific MicroRNAs. Dev Cell 2003;5:351–358.

45 Sharma A, Wu JC. MicroRNA expression profiling of human-induced pluripotent and embryonic stem cells. Methods Mol Biol 2013; 936:247–256.

46 Boyerinas B, Park SM, Hau A et al. The role of let-7 in cell differentiation and cancer. Endocr Relat Cancer 2010;17:F19–F36.

47 Kevany BM, Palczewski K. Phagocytosis of retinal rod and cone photoreceptors. Physiology (Bethesda) 2010;25:8–15.

48 Sparrow JR, Hicks D, Hamel CP. The retinal pigment epithelium in health and disease. Curr Mol Med 2010;10:802–823.

49 Seo JB, Moody M, Koh DS. Epithelial monolayer culture system for real-time single-cell analyses. Physiol Rep 2014;2:e12002.

50 Sanderson J, Dartt DA, Trinkaus-Randall V et al. Purines in the eye: Recent evidence for the physiological and pathological role of purines in the RPE, retinal neurons, astrocytes, Müller cells, lens, trabecular meshwork, cornea and lacrimal gland. Exp Eye Res 2014;127: 270–279.

51 Mitchell CH. Release of ATP by a human retinal pigment epithelial cell line: Potential for autocrine stimulation through subretinal space. J Physiol 2001;534:193–202.

52 Singh R, Shen W, Kuai D et al. iPS cell modeling of Best disease: Insights into the pathophysiology of an inherited macular degeneration. Hum Mol Genet 2013;22:593–607.

53 Singh R, Phillips MJ, Kuai D et al. Functional analysis of serially expanded human iPS cell-derived RPE cultures. Invest Ophthalmol Vis Sci 2013;54:6767–6778.

54 Ferrer M, Corneo B, Davis J et al. A multiplex high-throughput gene expression assay to simultaneously detect disease and functional markers in induced pluripotent stem cell-derived

retinal pigment epithelium. STEM CELLS TRANSLATIONAL MEDICINE 2014;3:911–922.

55 Steinberg RH. Monitoring communications between photoreceptors and pigment epithelial cells: effects of "mild" systemic hypoxia. Friedenwald lecture. Invest Ophthalmol Vis Sci 1987;28:1888–1904.

56 Rymer J, Miller SS, Edelman JL. Epinephrine-induced increases in [Ca2+](in) and KCl-coupled fluid absorption in bovine RPE. Invest Ophthalmol Vis Sci 2001;42:1921–1929.

57 Quinn RH, Quong JN, Miller SS. Adrenergic receptor activated ion transport in human fetal retinal pigment epithelium. Invest Ophthalmol Vis Sci 2001;42:255–264.

58 Nasu A, Ikeya M, Yamamoto T et al. Genetically matched human iPS cells reveal that propensity for cartilage and bone differentiation differs with clones, not cell type of origin. PLoS One 2013;8:e53771.

59 Hartjes KA, Li X, Martinez-Fernandez A et al. Selection via pluripotency-related transcriptional screen minimizes the influence of somatic origin on iPSC differentiation propensity. STEM CELLS 2014;32:2350–2359.

60 Rajamani K, Li YS, Hsieh DK et al. Genetic and epigenetic instability of stem cells. Cell Transplant 2014;23:417–433.

61 Hussein SM, Batada NN, Vuoristo S et al. Copy number variation and selection during reprogramming to pluripotency. Nature 2011; 471:58–62.

62 Koehler KR, Tropel P, Theile JW et al. Extended passaging increases the efficiency of neural differentiation from induced pluripotent stem cells. BMC Neurosci 2011;12:82.

63 Nazor KL, Altun G, Lynch C et al. Recurrent variations in DNA methylation in human pluripotent stem cells and their differentiated derivatives. Cell Stem Cell 2012;10:620–634.

64 Mekhoubad S, Bock C, de Boer AS et al. Erosion of dosage compensation impacts human iPSC disease modeling. Cell Stem Cell 2012;10: 595–609.

65 Hu Q, Friedrich AM, Johnson LV et al. Memory in induced pluripotent stem cells: Reprogrammed human retinal-pigmented epithelial cells show tendency for spontaneous redifferentiation. STEM CELLS 2010;28: 1981–1991.

66 Kajiwara M, Aoi T, Okita K et al. Donor-dependent variations in hepatic differentiation from human-induced pluripotent stem cells. Proc Natl Acad Sci USA 2012;109: 12538–12543.

67 Ryan JS, Baldridge WH, Kelly ME. Purinergic regulation of cation conductances and intracellular Ca2+ in cultured rat retinal pigment epithelial cells. J Physiol 1999;520: 745–759.

See www.StemCellsTM.com for supporting information available online.